PHYSICAL REVIEW B **96**, 241410(R) (2017)

Deterministic entanglement between a propagating photon and a singlet-triplet qubit in an optically active quantum dot molecule

Y. L. Delley,[1] M. Kroner,[1] S. Faelt,[1,2] W. Wegscheider,[2] and A. İmamoğlu[1]
[1]*Institute for Quantum Electronics, ETH Zürich, CH-8093 Zurich, Switzerland*
[2]*Laboratory for Solid State Physics, ETH Zürich, CH-8093 Zurich, Switzerland*
(Received 29 March 2017; revised manuscript received 13 November 2017; published 21 December 2017)

Two-electron charged self-assembled quantum dot molecules exhibit a decoherence-avoiding singlet-triplet qubit subspace and an efficient spin-photon interface. We demonstrate quantum entanglement between emitted photons and the spin qubit after the emission event. We measure the overlap with a fully entangled state to be $69.5 \pm 2.7\%$, exceeding the threshold of 50% required to prove the nonseparability of the density matrix of the system. The photonic qubit is encoded in two photon states with an energy difference larger than the timing resolution of existing detectors. We devise a heterodyne detection method, enabling the projective measurements of such photonic color qubits along any direction on the Bloch sphere.

DOI: 10.1103/PhysRevB.96.241410

Spins in optically active quantum dots (QDs) exhibit relatively short T_2^* coherence times. Despite this strong limitation, QDs stand out among solid-state qubit systems for their excellent optical properties that render them promising for quantum communication tasks relying on a quantum interface between stationary (spin) and flying (photonic) qubits. Recent experiments have used this favorable feature to demonstrate coherent all-optical spin manipulation [1], emission of entangled photon pairs [2,3], spin-photon entanglement [4–6], teleportation from a photonic to a spin qubit [7] and heralded distant spin entanglement using QDs in Voigt geometry [8]. However, the magnetic field configuration to achieve efficient spin measurement [9] is incompatible with the configuration for coherent manipulation.

The molecular states $|S\rangle$ and $|T_0\rangle$ in optically active quantum dot molecules (QDMs) in Faraday geometry [energy-level diagram in Fig. 1(a)] emerge as a promising alternative effective qubit for quantum information processing. (i) They exhibit a decoherence-avoiding clock transition that is insensitive to fluctuations in both electric and magnetic fields [10]. (ii) The spin-polarized triplet states ($|T_+\rangle$ and $|T_-\rangle$) of the ground-state manifold exhibit cycling optical transitions, which can scatter many photons without destroying the state, thus enabling a high-fidelity state readout [11]. (iii) The qubit states exhibit an equal coupling strength to common optically excited trion states, essential for maximal spin-photon entanglement. In this Rapid Communication, we experimentally determine the amount of entanglement obtained from the spontaneous emission from such an excited state.

S-T_0 qubits in QDMs. Our experiment is carried out on a single InGaAs self-assembled QDM, consisting of two vertically stacked QDs separated by a 9-nm GaAs tunneling barrier along the growth direction [12]. The QDM is embedded in a Schottky diode, formed by a semitransparent metallic top gate and an *n*-doped layer, which is used to control the charge state of the QDM and the optical transition energies via the quantum confined Stark effect [13]. A distributed Bragg reflector (DBR) below the doped layer forms a weak planar microcavity together with the top gate, enhancing the collection efficiency though a combination of emission profile modification and Purcell effect [9]. Owing to the engineered confinement energies of the two QDs, the QDM can be charged with a single electron in each of the QDs, the so-called (1,1) regime [14,15]. In this regime, the singlet state ($|S\rangle$) is split from the triplet states ($|T_0\rangle$, $|T_+\rangle$, and $|T_-\rangle$) by the exchange splitting, which is gate-voltage tunable and has a minimum value of $J = 97$ GHz in our device. The triplet states are split by 15.5 GHz from each other by an external magnetic field of 2 T that is applied along the growth direction (Faraday geometry). The relevant level scheme is outlined in Fig. 1(a). Under these conditions, $|S\rangle$ and $|T_0\rangle$ can be compared to atomic clock transitions that are insensitive to both electric and magnetic field fluctuations [10]. Coupling to the common optically excited state $|R_+\rangle$ (with equal oscillator strength) allows for coherent manipulation of the qubit [14,15]. The spontaneous radiative recombination of $|R_+\rangle$ projects the joint system of the QDM and the optical field into an entangled state,

$$|\Psi\rangle = \frac{1}{\sqrt{2}}(|S\rangle|b\rangle - |T_0\rangle|r\rangle), \tag{1}$$

where $|b\rangle$ and $|r\rangle$ denote single-photon states with center frequencies of ω_b and ω_r, respectively. Both of them are circularly polarized with the same handedness. The relative phase of the state is fixed by the optical selection rules.

Experimental setup. Figure 2 shows schematically how the experiment is set up. The sample is held in a liquid helium bath cryostat at about 5 K. A confocal microscope with a numerical aperture NA = 0.68 is used to direct ns pulses from tunable diode lasers to the QDM to manipulate the qubit state and to read it out via detection of resonance fluorescence (RF). The laser pulses are linearly polarized, and the RF is collected from the orthogonal linear polarization, such that all transitions couple to excitation and detection equally well [16,17], while the reflected laser light is suppressed by a factor of 10^6. Multiple Si avalanche photodiodes (APDs) are used to detect the emitted photons, and a time-digital converter (TDC) records the arrival time of every photon.

Entanglement generation and verification. Resonant laser pulses are used to initialize the QDM into $|S\rangle$ via optical spin pumping [18]. To this end, we combine the light of two lasers. One laser is simultaneously resonant with the optical transitions $|T_0\rangle \leftrightarrow |R_+\rangle$ and $|T_+\rangle \leftrightarrow |R_{++}\rangle$, and the other laser

 ©2017 American Physical Society

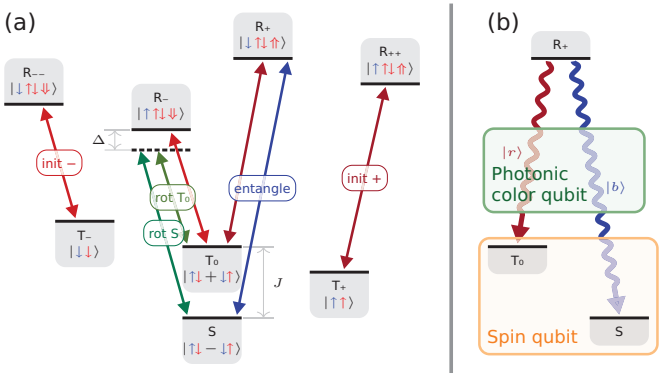

FIG. 1. (a) Spin states and optically excited states in the (1,1) regime. In each state label, the upper row denotes the state name that we use in the main text, and the lower row expresses the state in terms of single particle states. There, single arrows denote electron spins, and double arrows denote heavy-hole spins. Only the lowest-lying orbital confined states are relevant. Spins denoted by a red (blue) arrow are mainly located in the top (bottom) dot. The exchange interaction $J \approx 97$ GHz splits the ground state into a singlet ($|S\rangle$) and triplets ($|T_-\rangle$, $|T_0\rangle$, and $|T_+\rangle$, further split by the magnetic field). Resonant laser fields create an electron-hole pair located in the top quantum dot with a lower-energy fundamental exciton transition energy; the corresponding optically excited states are denoted by $|R_{--}\rangle$, $|R_-\rangle$, $|R_+\rangle$, and $|R_{++}\rangle$. The excitonic transitions in the bottom dot with stronger confinement are much higher in energy and do not couple to the applied laser fields. The transitions are labeled with the name of the laser that drives them. "init+" is simultaneously resonant with $|T_0\rangle \leftrightarrow |R_+\rangle$ and $|T_+\rangle \leftrightarrow |R_{++}\rangle$, while "init−" is simultaneously resonant with $|T_0\rangle \leftrightarrow |R_-\rangle$ and $|T_-\rangle \leftrightarrow |R_{--}\rangle$. They are used to pump the spin into $|S\rangle$, as well as to measure the population in $|T_0\rangle$. "Entangle" excites $|R_+\rangle$ from $|S\rangle$, as well as is used to measure the population in $|S\rangle$. "rot T_0" and "rot S" induce a coherent spin rotation, and are red detuned by Δ from $|T_0\rangle \leftrightarrow |R_-\rangle$ and $|S\rangle \leftrightarrow |R_-\rangle$, respectively. (b) The effective spin qubit is made up of the states $|S\rangle$ and $|T_0\rangle$. Decay from the excited state $|R_+\rangle$ projects the spin into an entangled state with the photonic color qubit in the space spanned by $|r\rangle$ and $|b\rangle$.

is simultaneously resonant with the transitions $|T_0\rangle \leftrightarrow |R_-\rangle$ and $|T_-\rangle \leftrightarrow |R_{--}\rangle$.

From $|S\rangle$, a 375-ps-long resonant laser pulse prepares the QDM in $|R_+\rangle$. Spontaneous emission creates the entangled state between the propagating photon and the remaining spin qubit in the $|S\rangle$-$|T_0\rangle$subspace.

To verify the entangled state, we estimate the overlap of the postemission state described by the density matrix $\hat{\rho}$ with the entangled state $|\Psi\rangle$ as defined in Eq. (1), quantified by the state fidelity

$$\begin{aligned} F &= \mathrm{Tr}(\hat{\rho}|\Psi\rangle\langle\Psi|) \\ &= \frac{1}{2}\underbrace{(\hat{\rho}_{Sb,Sb} + \hat{\rho}_{T_0r,T_0r})}_{F_\parallel} \\ &\quad - \frac{1}{2}\underbrace{(\hat{\rho}_{Sb,T_0r} + \hat{\rho}_{T_0r,Sb})}_{F_\perp}. \end{aligned} \tag{2}$$

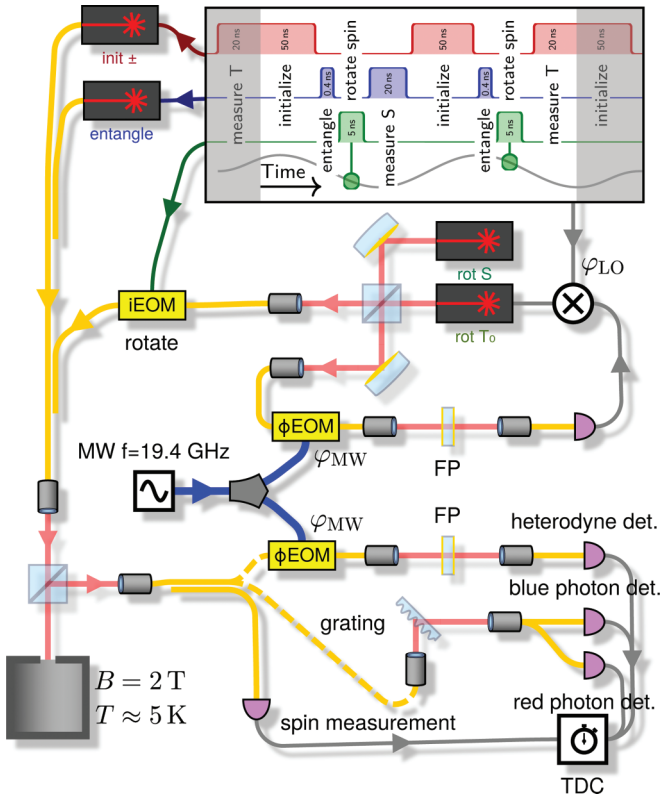

FIG. 2. Inset: Pulse sequence for the measurement of quantum correlations. Each cycle performs two entanglements, with the spin measured once in $|S\rangle$ and once in $|T_0\rangle$. The phase φ_{LO} changes with each repetition. The measurement of classical correlations is analogous, leaving out the rotation pulse. Main figure: Schematic of the experimental setup. TDC: Time-to-digital converter. iEOM: Electro-optic intensity modulator. ΦEOM: Electro-optic phase modulator. FP: Fabry-Pérot étalon. MW: Microwave source. The cw lasers are gated using iEOMs to generate ns pulses. Details of the pulse generation for the lasers init+, init−, and entangle are left out for clarity. The ΦEOMs mix a MW signal into the photons to enable phase relationship measurements between different wavelengths. Classical correlations and quantum correlations are measured in separate experiments; only one fiber (dashed in the schematic) of the two corresponding photon-detection setups is connected at a time, while the other is disconnected.

The fidelity can be decomposed into two parts: $F_\parallel$ quantifies the amount of *classical* correlations between the probabilities of finding each subsystem in a particular eigenstate. $F_\perp$, on the other hand, is sensitive to the relative phase between the two parts of the state $|\Psi\rangle$ when written in the eigenbasis, thus we refer to that term as the *quantum* correlations. The state described by $\hat{\rho}$ generally is a mixture of pure states, such that F becomes a convex mixture of the fidelity of each contained pure state. Since no separable state has a higher fidelity than $1/2$, observing a fidelity above that limit proves inseparability of $\hat{\rho}$ [19].

Measurement of the classical correlations. To estimate $F_\parallel$, we measure the correlations between the two subsystems in their eigenbases. To that end, we disperse the photon from the entanglement pulse using a transmission grating, split the two-color components using a fiber bundle with two cores

next to each other, and detect it using a dedicated APD for each component.

To measure the spin, we detect the scattered photons from spin-selective RF [20], where either a laser pulse resonant with $|S\rangle \leftrightarrow |R_+\rangle$ is used to detect the state $|S\rangle$, or a combined two-laser pulse resonant with $|T_0\rangle \leftrightarrow |R_+\rangle$ and $|T_0\rangle \leftrightarrow |R_-\rangle$ is used to detect the state $|T_0\rangle$. Contrary to spin initialization, for spin measurement, any one of the two lasers would suffice. However, that would have required an additional EOM and a pulse-pattern channel, neither of which were easily available.

Figures 3(a) and 3(b) show the time-resolved fluorescence measured by the spectrally filtered detectors, conditioned on the observation of a photon during the following spin measurement pulse. We normalized the values using the relative overall sensitivity of the two detection paths, which we determined separately [21]. There is a strong correlation between the spin and the detected photon color: $P(b|S) : P(r|S) = (90.1 : 9.9)\pm 1.0\%$ and $P(b|T_0) : P(r|T_0) = (10.2 : 89.8)\pm 0.9\%$. Here, $P(p|s)$ denotes the probability to detect a photon in state $p \in \{r,b\}$, conditioned on the successful detection of the spin in state $s \in \{S,T_0\}$. Errors are one standard deviation and are derived from counting statistics. We take $P(b) + P(r) = 1$ as well as $P(S) + P(T) = 1$, valid if the results are conditioned to the cases where a photon is detected, and as long as optically forbidden transitions are rare. From this, we can extract a lower bound to the fidelity as $F_\parallel = [P(b|S)P(S) + P(r|T_0)P(T_0)] \geqslant \min\{P(b|S), P(r|T_0)\} = 89.4 \pm 0.8\%$ since $F_\parallel$ is a convex mixture of the two conditional probabilities.

We attribute the reduction from perfect correlations mainly to double excitation during the entanglement pulse: The duration of the excitation pulse is comparable with the exciton lifetime of about 400 ps, such that emission events early during the pulse may lose the correlation with the spin during subsequent excitation events. Simulation of the optical Bloch equations suggest between 5% and 10% double-excitation events.

Measurement of quantum correlations. To determine $F_\perp$, we measure both the photon and the spin in a superposition basis, where the basis states are lying on the equator of Bloch spheres of the subsystems. Entanglement between the systems then implies a sinusoidal dependency of coincidence probabilities on the relative azimuthal angle between each system's measurement basis [22].

To measure the photon in a superposition state of the two colors, we need to detect the phase of the beat note at $\omega_J = 2\pi \cdot 97$ GHz. This is faster than the timing resolution of existing photodetectors. We therefore employ a heterodyne detection scheme: Using an electro-optic phase modulator (phase-EOM) driven by a microwave (MW) signal, we generate sidebands to each spectral component of the incoming photon. The MW frequency ω_{MW} is close to ω_J divided by an integer; due to the limitations of our MW source, we chose $\omega_J/5$. A free-space Fabry-Pérot étalon with a free spectral range of 200 GHz and a bandwidth of 5 GHz allows us to single out the $k = +3$ sideband of the red photon simultaneously with the $k = -2$ sideband of the blue photon (see Fig. S2 in the Supplemental Material [21]). These two sidebands interfere constructively or destructively with each other, depending on the relative phase of the incoming photon components and the MW phase φ_{MW}.

The quantum action $\hat{S}_{\mathrm{PM}}$ of a phase modulator driven by a coherent MW state with average modulation amplitude V_m and phase φ_{MW} onto a single photon of frequency ω in the optical regime can be approximated to excellent precision as [23]

$$\hat{S}^\dagger_{\mathrm{PM}}|1_\omega\rangle \approx \sum_{k=-\lfloor\omega/\omega_{\mathrm{MW}}\rfloor}^{\infty} (-ie^{-i\varphi_{\mathrm{MW}}})^k J_k(V_m)|1_{\omega+k\omega_{\mathrm{MW}}}\rangle,$$

up to a constant propagation phase. Here, k denotes the sideband order and J_k are Bessel functions of the first kind. Photons emitted by the QDM can be described in the standard continuous-mode formalism as wave packets of the form

$$|r,b\rangle = \int_0^\infty d\omega\, f(\omega - \omega_d)|\omega\rangle.$$

Here, f is normalized and describes the limited-bandwidth spectrum of a spontaneously emitted photon. Furthermore, in the single-photon subspace, detection of a photon at time $t \approx 0$ using a detector that is band limited around ω_d can be described by the operator $|d\rangle\langle d|$, with the wave packet $|d\rangle$ described by

$$|d\rangle = \int_0^\infty d\omega\, g(\omega - \omega_d)|\omega\rangle.$$

where g describes the spectral window of the detector.

For a photon in a pure two-color state $\alpha|r\rangle + \beta|b\rangle$, if the bandwidth of the convolution of the spectral functions f and g is smaller than the modulation frequency ω_{MW}, at most one sideband of each color component contributes to the detection probability. With the parameters used in our experiment, the detection probability for the above two-color photon is thus given by

$$\begin{aligned} p &= |\langle d|S^\dagger_{\mathrm{PM}}[\alpha|r\rangle + \beta|b\rangle]|^2 \\ &= \left|\int_{-\omega_d}^\infty d\delta\, g^*(\delta)[\alpha i e^{-3i\varphi_{\mathrm{MW}}} J_3(V_m) f(\delta + 3\Delta) \right. \\ &\qquad \left. - \beta e^{2i\varphi_{\mathrm{MW}}} J_{-2}(V_m) f(\delta - 2\Delta)]\right|^2, \\ &= |\alpha u_r + \beta u_b e^{5i\varphi_{\mathrm{MW}}}|^2, \end{aligned}$$

where $\delta = \omega - \omega_d$ is the optical detuning from the filter center, $\Delta = \omega_J/5 - \omega_{\mathrm{MW}}$ is the detuning of the MW frequency, and $u_{r,b}$ are complex numbers resulting from the overlap integral between f and g. By adjusting the filter and the modulation depth, the latter can be made equal. In that case, detection of a photon after the étalon corresponds to a projective measurement described by the partial trace

$$\mathrm{Tr}_{(\mathrm{phot})}\{\hat{\rho}[1 + (e^{5i\varphi_{\mathrm{MW}}}|r\rangle\langle b| + \mathrm{H.c.})]\}, \tag{3}$$

where $\hat{\rho}$ describes a general incoming single photon. Thus, the phase of the detection basis $|r\rangle \pm e^{5i\varphi_{\mathrm{MW}}}|b\rangle$ is determined only by the MW source phase φ_{MW}. In the rotating frame of the two-color photon, this phase rotates at a frequency of $5\omega_{\mathrm{MW}} - \omega_J \approx 0$, which can be chosen arbitrarily. It was set to 131 MHz, such that the timing jitter of standard Si-APDs does not affect the measured visibility.

To measure the spin in a superposition state, we rotate the spin by $\pi/2$ around a vector in the equatorial plane of the Bloch sphere, and then measure the population in the $|S\rangle$ or $|T_0\rangle$ states

via RF detection. To that end, we utilize a variation of the standard method of ultrafast coherent optical control based on the optical (ac-) Stark effect (see Ref. [24] and references therein): Instead of using a single ps pulse that is far detuned from both transitions, we use two quasiresonant ns pulses detuned by $\Delta \approx 10$ GHz from the transitions $|S\rangle \leftrightarrow |R_-\rangle$ and $|T_0\rangle \leftrightarrow |R_-\rangle$ to induce an energy shift to a coherent superposition state $[e^{-i\varphi_S}|S\rangle + e^{-i\varphi_T}|T_0\rangle]/\sqrt{2}$. By adjusting the pulse length and power to a rotation angle of $\phi_{\rm rot} = \int dt|\Omega(t)|^2/\Delta = \pi/2$, the pulse maps $[e^{-i\varphi_S}|S\rangle \pm ie^{-i\varphi_T}|T_0\rangle]/\sqrt{2}$ to $|S\rangle$ (for "+") and $|T_0\rangle$ (for "−"). Thus, the azimuthal angle of the rotation vector is determined by the phase difference $\varphi_S - \varphi_T$ of the two laser pulses, which stays constant during the pulse in the rotating frame of the spin. To ensure a fixed phase relation over the whole measurement time, we embed one of the two diode lasers in a phase-locked loop (PLL), relying on the same heterodyne detection method employed for the photon measurement: The 97-GHz beat note of the two lasers is down mixed via sideband generation and spectral filtering, where the MW signal is derived from the same source that drives the photon measurement. The resulting beat note of 131 MHz is then phase locked to a local oscillator (LO) that is synchronized with the pulse sequence, ensuring $\varphi_S - \varphi_T - 5\varphi_{\rm MW} = \varphi_{\rm LO}$. Spin detection in $|S\rangle$ or $|T_0\rangle$ after a $\pi/2$ rotation hence corresponds to a projective measurement described by the partial trace

$$\mathrm{Tr}_{(\mathrm{spin})}\{\hat{\rho}[1 \pm (e^{i(5\varphi_{\rm MW}+\varphi_{\rm LO})}|S\rangle\langle T_0| + \mathrm{H.c.})]\}, \qquad (4)$$

with the sign depending on the state the spin is detected in.

With this detection scheme, given an arbitrary joint density matrix $\hat{\rho}$, the probability to detect a coincidence between the photon measurement and the spin measurement can be found by combining (3) and (4) to

$$\begin{aligned} P_{\rm co} \propto\ & \mathrm{Tr}\{\hat{\rho}[1 + (e^{5i\varphi_{\rm MW}}|r\rangle\langle b| + \mathrm{H.c.})] \\ & \times [1 \pm (e^{i(5\varphi_{\rm MW}+\varphi_{\rm LO})}|S\rangle\langle T_0| + \mathrm{H.c.})]\} \\ =\ & 1 \pm \mathcal{R}[e^{i\varphi_{\rm LO}}\hat{\rho}_{Sb,T_0r} + e^{10i\varphi_{\rm MW}}\hat{\rho}_{Sr,T_0b} \\ & \pm e^{5i\varphi_{\rm MW}}(\hat{\rho}_{Sb,Sr} + \hat{\rho}_{T_0b,T_0r}) \\ & + e^{i(5\varphi_{\rm MW}+\varphi_{\rm LO})}(\hat{\rho}_{Sr,T_0r} + \hat{\rho}_{Sb,T_0b})]. \end{aligned}$$

By letting the MW source run freely, we average over $\varphi_{\rm MW}$, such that the modulation depth of the coincidence rate with respect to $\varphi_{\rm LO}$ is a direct measure of $F_\perp$. Figures 3(c) and 3(d) show the detected photon counts conditioned on detection of a scattered photon during the spin measurement, depending on the phase $\varphi_{\rm LO}$. By fitting a sinusoidal function to the data, we extract the modulation depth (the amplitude of the sine relative to the mean value) of the measured coincidence rate. When the spin is measured in the $|S\rangle$ state, the observed modulation depth is $45.0 \pm 3.3\%$, and $49.0 \pm 3.3\%$ when the spin is measured in the $|T_0\rangle$ state. Errors are one standard deviation and are derived from counting statistics. Since imperfections in the measurement process can only reduce the modulation depth, the higher value of the two puts a lower bound on $F_\perp \geqslant \max\{v_S, v_{T_0}\} = 49.5 \pm 2.9\%$.

This value is considerably lower than the ideal case for perfect entanglement, where we would expect 100% visibility. A significant amount of visibility is lost due to the spectral filtering properties of the Fabry-Pérot étalon used in the phase-sensitive photon detection setup, limiting the visibility of the $F_\perp$ measurement to about 84%: The beating of neighboring pairs of sidebands are out of phase by π. Our FP étalon

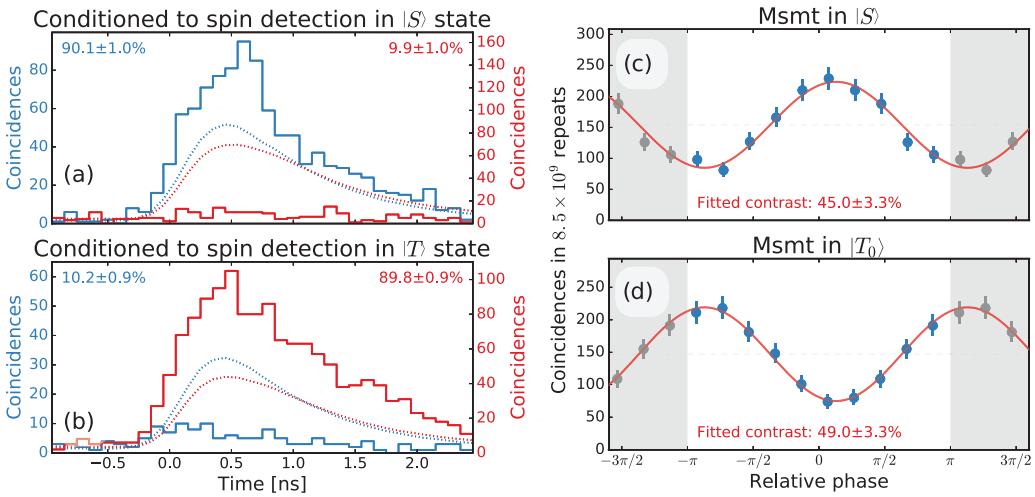

FIG. 3. (a) Solid lines: Histogram of coincidences between spin detection in the $|S\rangle$ state and photon color detected to be $|\omega_r\rangle$ (red line) and $|\omega_b\rangle$ (blue line). Dotted lines: Expected coincidence counts from individual detection rates, disregarding spin measurement. The two photon colors have separate vertical scales to account for the different sensitivities of the two detection paths. (b) As (a), but spin detection in the $|T_0\rangle$ state. Both data sets were measured simultaneously, and are histogrammed from 2.7×10^{10} repetitions each, acquired over a time period of about 12 h. (c), (d) Dots and bars: Total number of coincidence events between the beat-phase-sensitive photon detector and postrotation measured spin in $|S\rangle$ and $|T_0\rangle$, respectively, plotted against the relative phase between the photon detection and the spin-rotation pulse. Vertical lines denote 68% confidence intervals derived from Poissonian statistics. Shaded areas outside the interval $[-\pi,\pi]$ contain replicas of the data points displayed inside this interval. Solid lines: Maximum-likelihood fit of a sinusoid to the data. Both data sets were simultaneously fitted with a fixed relative phase shift of π, but individual mean and amplitude.

only suppresses the neighboring pairs by a factor of 12 (see Supplemental Material [21] for the spectral selectivity of the Fabry-Pérot étalon). The limitation can be overcome by using higher finesse FPs or higher MW frequencies. A further reduction of the visibility is likely to be due to imperfections of the spin-rotation pulse. (See the Supplemental Material [21] for a detailed listing of all sources of error).

Combining the two measurements, we obtain $F = 69.5 \pm 2.7\%$, where the error indicates one standard deviation of uncertainty due to counting statistics.

To summarize, we have shown deterministic generation of a photonic color qubit entangled with the QDM spin qubit. Working with color qubits split by a large energy separation was enabled owing to our heterodyne quadrature detection method, effectively erasing the energy separation. Since the $|S\rangle$-$|T_0\rangle$ spin qubit can controllably be furnished with a dipole, QDMs promise to bridge the gap between optical long-distance quantum communication and quantum information processing in the solid state. Possible candidates for coupling to the QDM dipole are (a) the dipole of quantum-well exciton (di)polaritons in planar microcavities [25], (b) the electric field of photons in microwave cavities [26], and (c) phonons of microresonators via the piezoelectricity of GaAs.

We acknowledge helpful discussions with Joseph M. Renes and Emre Togan. This work is supported by NCCR Quantum Science and Technology (NCCR QSIT), research instrument of the Swiss National Science Foundation (SNSF), and by Swiss NSF under Grant No. 200021-140818.

[1] D. Press, K. De Greve, P. L. McMahon, T. D. Ladd, B. Friess, C. Schneider, M. Kamp, S. Hofling, A. Forchel, and Y. Yamamoto, Nat. Photonics **4**, 367 (2010).

[2] R. J. Young, R. M. Stevenson, A. J. Shields, P. Atkinson, K. Cooper, and D. A. Ritchie, J. Appl. Phys. **101**, 081711 (2007).

[3] R. Hafenbrak, S. M. Ulrich, P. Michler, L. Wang, A. Rastelli, and O. G. Schmidt, New J. Phys. **9**, 315 (2007).

[4] W. B. Gao, P. Fallahi, E. Togan, J. Miguel-Sanchez, and A. Imamoglu, Nature (London) **491**, 426 (2012).

[5] K. De Greve, L. Yu, P. L. McMahon, J. S. Pelc, C. M. Natarajan, N. Y. Kim, E. Abe, S. Maier, C. Schneider, M. Kamp, S. Hofling, R. H. Hadfield, A. Forchel, M. M. Fejer, and Y. Yamamoto, Nature (London) **491**, 421 (2012).

[6] J. R. Schaibley, A. P. Burgers, G. A. McCracken, L.-M. Duan, P. R. Berman, D. G. Steel, A. S. Bracker, D. Gammon, and L. J. Sham, Phys. Rev. Lett. **110**, 167401 (2013).

[7] W. B. Gao, P. Fallahi, E. Togan, A. Delteil, Y. S. Chin, J. Miguel-Sanchez, and A. Imamoğlu, Nat. Commun. **4**, 2744 (2013).

[8] A. Delteil, Z. Sun, W.-b. Gao, E. Togan, S. Faelt, and A. Imamoğlu, Nat. Phys. **12**, 218 (2016).

[9] A. Delteil, W.-b. Gao, P. Fallahi, J. Miguel-Sanchez, and A. İmamoğlu, Phys. Rev. Lett. **112**, 116802 (2014).

[10] K. M. Weiss, J. M. Elzerman, Y. L. Delley, J. Miguel-Sanchez, and A. İmamoğlu, Phys. Rev. Lett. **109**, 107401 (2012).

[11] Y. L. Delley, M. Kroner, S. Faelt, W. Wegscheider, and A. İmamoğlu, arXiv:1509.04171.

[12] Q. Xie, A. Madhukar, P. Chen, and N. P. Kobayashi, Phys. Rev. Lett. **75**, 2542 (1995).

[13] D. A. B. Miller, D. S. Chemla, T. C. Damen, A. C. Gossard, W. Wiegmann, T. H. Wood, and C. A. Burrus, Phys. Rev. Lett. **53**, 2173 (1984).

[14] D. Kim, S. G. Carter, A. Greilich, A. S. Bracker, and D. Gammon, Nat. Phys. **7**, 223 (2011).

[15] A. Greilich, S. G. Carter, D. Kim, A. S. Bracker, and D. Gammon, Nat. Photonics **5**, 702 (2011).

[16] A. N. Vamivakas, C. Y. Lu, C. Matthiesen, Y. Zhao, S. Falt, A. Badolato, and M. Atature, Nature (London) **467**, 297 (2010).

[17] S. T. Yılmaz, P. Fallahi, and A. İmamoğlu, Phys. Rev. Lett. **105**, 033601 (2010).

[18] M. Atatüre, J. Dreiser, A. Badolato, A. Högele, K. Karrai, and A. Imamoglu, Science **312**, 551 (2006).

[19] C. A. Sackett, D. Kielpinski, B. E. King, C. Langer, V. Meyer, C. J. Myatt, M. Rowe, Q. A. Turchette, W. M. Itano, D. J. Wineland, and C. Monroe, Nature (London) **404**, 256 (2000).

[20] A. N. Vamivakas, Y. Zhao, C.-Y. Lu, and M. Atatüre, Nat. Phys. **5**, 198 (2009).

[21] See Supplemental Material at http://link.aps.org/supplemental/10.1103/PhysRevB.96.241410 for data from characterisation measurements of the experimental setup, as-well as an estimation of the impact on the measured fidelity of all known sources of imperfection.

[22] B. B. Blinov, D. L. Moehring, L.-M. Duan, and C. Monroe, Nature (London) **428**, 153 (2004).

[23] J. Capmany and C. R. Fernández-Pousa, J. Phys. B: At., Mol. Opt. Phys. **44**, 035506 (2011).

[24] D. Press, T. D. Ladd, B. Zhang, and Y. Yamamoto, Nature (London) **456**, 218 (2008).

[25] G. Christmann, A. Askitopoulos, G. Deligeorgis, Z. Hatzopoulos, S. I. Tsintzos, P. G. Savvidis, and J. J. Baumberg, Appl. Phys. Lett. **98**, 081111 (2011).

[26] Y. Tsuchimoto, P. Knüppel, and A. Imamoğlu Phys. Rev. B **96**, 165312 (2017).